

ENHANCED DETECTION OF TINY OBJECTS IN AERIAL IMAGES

Kihyun Kim^{*1} Michalis Lazarou² Tania Stathaki¹
yoo07220@gmail.com michalislazarou93@gmail.com t.stathaki@imperial.ac.uk

¹ Dept. of Electrical & Electronic Engineering, Imperial College London

² Center for Vision, Speech and Signal Processing, University of Surrey

ABSTRACT

While one-stage detectors like YOLOv8 offer fast training speed, they often under-perform on detecting small objects as a trade-off. This becomes even more critical when detecting tiny objects in aerial imagery due to low-resolution targets and cluttered backgrounds. To address this, we introduce four enhancement strategies—*input image resolution adjustment, data-augmentation, attention mechanisms and an alternative gating function for attention modules*—that can be easily implemented on YOLOv8. We demonstrate that image size enlargement and the proper use of augmentation can lead to enhancement. Additionally, we designed a **Mixture of Orthogonal Neural-modules Network (MoonNet)** pipeline which consists of multiple attention modules-augmented CNNs. Two well-known attention modules Squeeze-and-Excitation (SE) Block and Convolutional Block Attention Modules (CBAM) were integrated into the backbone of YOLOv8 to form MoonNet design and the MoonNet backbone obtained improved detection accuracy compared to the original YOLOv8 backbone and the single-type attention modules-augmented backbone. MoonNet further proved its adaptability and potential by achieving state-of-the-art performance on the tiny-object benchmark when integrated with the YOLC model. Our code is available at: <https://github.com/Kihyun11/MoonNet>

Index Terms— Tiny object detection, Deep learning, Attention mechanism, YOLO

1. INTRODUCTION

Advances in deep learning have transformed object detection, evolving from early sliding-window CNNs such as R-CNN [1] to modern pyramidal, end-to-end architectures. Two-stage detectors—including Faster R-CNN [2], Feature Pyramid Networks (FPN) [3], and Mask R-CNN [4]—first generate region proposals and then refine classification and localization, achieving state-of-the-art accuracy. In parallel, one-stage models prioritize speed by eliminating the proposal stage; seminal examples include SSD [5] and the “You Only Look Once” (YOLO) family [6] [7]. Although one-stage

detectors excel in training speed, they tend to struggle with detecting tiny objects as a design trade-off. This limitation is especially pronounced in aerial imagery, where targets often occupy only a few pixels amid cluttered backgrounds. Many studies have been conducted to tackle this problem and delivered significant enhancement using YOLO model family. Our research is highly influenced by both Zhu et al [8] and Kang et al [9] which successfully demonstrated the detection accuracy gain in aerial images using the attention modules. Kang et al. especially show that their multiple attention module augmented architecture is better than the SE Block-Only architecture. We further extended this idea to investigate whether the mixed use of attention modules can be always beneficial and what other factors can play an important role in detecting tiny objects using YOLOv8 and YOLC framework. Our contributions are fourfold: (i) effectiveness of higher input resolution, (ii) importance of targeted data augmentation, (iii) compare a hybrid attention-augmented backbone against the single-type attention augmented backbone and obtain the MoonNet design which out-performed among the design candidates, and (iv) suggest a possible alternative gating mechanism for attention modules.

2. RELATED WORK

Tiny object detection in general: Prior work has explored various methods for tiny object detection. Xu et al. [10] suggest that effective enhancement methods for tiny object detection can be categorized into five: *multi-scale feature learning, context-based detection, data augmentation, designing better training strategy and label assignment strategy*. High resolution imagery is crucial as well and numerous approaches were made to improve the resolution of the images such as Query-Det [11]. Some studies such as YOLC [12] even use cropping method to make the training more efficient.

Input image resolution: Yan et al. [13] demonstrated that increasing the input image resolution can significantly improve the detection of small-scale objects, as it enables the model to capture more detailed features. Motivated by this, we experiment with multiple input image resolutions in this study to assess their impact.

^{*}Thanks to Hyesoon Kim and Seonhwan Kim for funding & support

Data Augmentation: Proper augmentation is critical when dealing with limited and highly imbalanced datasets. Kisantal et al. [14] identified the scarcity of images containing tiny objects and their limited representation in the dataset as a major challenge for small object detection. They addressed this issue using a copy-paste augmentation strategy.

Attention Module & Gating Function: Hu et al. [15] proposed the Squeeze-and-Excitation (SE) block to enhance CNNs by modeling inter-channel dependencies and recalibrating feature responses. Woo et al. [16] extended this with the Convolutional Block Attention Module (CBAM), which combines channel and spatial attention to better focus on informative regions—an advantage in tiny object detection where spatial precision is crucial. Both modules use sigmoid as a gating function to allow the model to focus on relevant features and avoid vanishing gradients.

Previous studies using YOLO: Plenty of research specifically targeting the enhancement of tiny object detection using the YOLO model already exists. Ma et al. [17] improve YOLOv8s for tiny-object detection by substituting standard strided convolutions with the SPD-Conv module and replacing the PANet neck with SPANet, achieving finer feature preservation and stronger multi-scale fusion. Hu et al. [18] enhance YOLOv5 through an Efficient Spatial Pyramid Pooling (ESPP) module, raising small-object accuracy in aerial imagery while keeping the network lightweight.

Relation to prior work: Implementation of attention modules on the YOLO architecture had been explored previously. Zhu et al. [8] introduces TPH-YOLO, which demonstrates the effectiveness of the CBAM with YOLOv5 architecture when detecting objects in aerial imagery. Kang et al.[9]’s SE-CBAM-YOLOv7 used both SE Block and CBAM modules on the YOLOv7’s architecture to detect tiny aircraft in aerial images. Unlike Zhu et al. and Kang et al., we focused more on testing several backbone designs with different attention module orientations to check the validity of using multiple attention modules and obtaining the best backbone candidate for enhancement.

We have also made an algorithmic modification on the SE Block and CBAM. As mentioned earlier, sigmoid is a commonly used gating function for the attention modules. A few other modules uses sigmoid as well, for instance, ECA-Module [19]. In this work, we tested a different gating mechanism $(1 + \tanh(\cdot))$, which is an identity safe gating that can preserve the original feature and also amplifies the scarce relevant features from tiny objects.

3. METHODOLOGY

3.1. Enhancement Strategy

In total, four different enhancement strategies were implemented on YOLOv8 to obtain efficient training.

Varying the input image resolution: Three different input image resolutions 640, 800, and 928 were tested.

Data Augmentation: A total of three different sets of data augmentation techniques were applied. The first set is the default augmentation setting provided by the Ultralytics. The second set is geometric transformations-focused package and the third set is color space adjustments-focused package. While these augmentations simulated real-world variations, the primary motivation was to mitigate class imbalance—particularly for under-represented tiny object classes.

Attention Modules Integration: To improve the model’s sensitivity to fine-grained details, attention modules were integrated into the YOLOv8 backbone. Specifically, Squeeze-and-Excitation (SE) blocks and Convolutional Block Attention Modules (CBAM) were inserted directly into select convolutional layers of the backbone. Instead of implementing them as standalone modules, the convolution layer class was extended to perform channel-wise recalibration (SE) and spatial attention (CBAM) inline.

Identity-safe gating mechanism: While attention modules are implemented on the backbone, the gating function is switched. Thus, one set of two backbones with the same attention module arrangement but different gating was trained and tested. The modifications are presented in Equations 1 and 2 and the full mathematical operations of SE Block and CBAM are available via Hu et al.[15] and Woo et al.[16]:

Squeeze-Excitation Operation (Ours)

$$y_{\text{original}} = x \odot \sigma(z), \quad \sigma = \text{sigmoid}, \quad (1a)$$

$$y_{\text{ours}} = x \odot (1 + \tanh(z)). \quad (1b)$$

CBAM Operation (Ours)

$$x_c^{\text{original}} = x \odot \sigma(z_c), \quad (2a)$$

$$x_c^{\text{ours}} = x \odot (1 + \tanh(z_c)), \quad (2b)$$

$$y_{\text{original}} = x_c^{\text{original}} \odot \sigma(z_s), \quad (2c)$$

$$y_{\text{ours}} = x_c^{\text{ours}} \odot (1 + \tanh(z_s)). \quad (2d)$$

Parameters & notes: Channel logits z (SE) and z_c (CBAM) lie in \mathbb{R}^C and are broadcast over $H \times W$ (equivalently reshape to $C \times 1 \times 1$). Spatial logits $z_s \in \mathbb{R}^{1 \times H \times W}$ are broadcast over channels. Here \odot denotes element-wise multiplication. x denotes the input feature map and the subscript c means channel-wise. All variables with the *original* subscript denote the original operation whereas that with *ours* denotes the modified operation.

Placement. For the YOLO-model, the modules were applied to the convolutional layers in the backbone. For the YOLC-model, the attention is applied *per branch at the outputs of the final HRNet stage* (post-branch adapters), not inside internal convolutional blocks. Let $\{f^{(i)}\}_{i=1}^B$ be the multi-resolution maps ($B=4$); we compute $y^{(i)} = \mathcal{A}^{(i)}(f^{(i)})$, $\mathcal{A}^{(i)} \in \{\text{SE BLOCK, CBAM}\}$. Because gating is multiplicative, tensor shapes and channels are unchanged, so the YOLC neck/head need no code changes.

3.2. Final Configuration

Following a multi-stage enhancement optimization process, the final model configuration was determined by selecting the most effective combinations of image resolution, data augmentation techniques, network architecture, and gating function. Using the modified backbone with integrated attention modules and the best-performing input image resolution setting, the final model was trained from scratch.

4. EXPERIMENTS AND RESULTS

4.1. Datasets

Modified DOTA2.0. We modified the original DOTA 2.0 dataset by selectively retaining only those object categories that consistently exhibit small spatial footprints in aerial imagery. The resulting modified dataset comprises five classes: *small vehicle*, *large vehicle*, *ship*, *plane*, and *storage tank*. Since the modified dataset was used, the evaluation could not be done through evaluation server but was performed locally using the validation set. The dataset is fully reproducible and the method is provided in the repository. Refer to Table 1, the retained objects occupy approximately **2214 pixels² (47×47)**.

VisDrone. We also evaluated on the VisDrone benchmark in Table 4 and Table 7 to assess generalization and enable fair comparison. Since the VisDrone server is currently unavailable, we used the validation set for evaluation.



Fig. 1: Object categories of the Modified-DOTA

Table 1: Pixel size comparison

Object Classes	Average pixel size
Small Vehicle	$\approx 1458 \text{ px}^2 (38 \times 38)$
Large Vehicle	$\approx 12407 \text{ px}^2 (111 \times 111)$
Ship	$\approx 1199 \text{ px}^2 (35 \times 35)$
Plane	$\approx 580 \text{ px}^2 (24 \times 24)$
Storage Tank	$\approx 2591 \text{ px}^2 (51 \times 51)$
Small Object Category Threshold	
COCO -"small" [20]	$1024 \text{ px}^2 (32 \times 32)$
Modified-DOTA (Ours)	$\approx 2214 \text{ px}^2 (47 \times 47)$

4.2. Training setting

YOLOv8: All the training runs were conducted on a local workstation equipped with an NVIDIA RTX 4080 SUPER GPU (16 GB VRAM). The environment ran Ultralytics 8.3.239, Python 3.9.10, and PyTorch 2.5.1 on CUDA 12.1

YOLOC: All the trainings were conducted in a secure cloud using one NVIDIA A40 GPU. The environment ran PyTorch 2.1.0, Python 3.10, and CUDA 11.8.0 on Ubuntu 22.04.

Trial screening: Input image adjustment, augmentation, and backbone testing were performed over 50 epochs (batch size 4, 640×640 image size) using the AdamW optimizer and a modified, default-augmented DOTA dataset. The trainings used a pretrained YOLOv8n-obb model.

Final training: The YOLOv8n-obb with the default and MoonNet backbones were trained for 150 epochs with batch size 4 and the selected candidates setting. The YOLOC model trainings were conducted for 50 epochs.

Evaluation metrics: Performance was evaluated using AP_{50} , AP , recall, and precision for YOLOv8; and AP_{50} , AP_{75} , and AP for YOLOC in MMDetection. AP_{50} and AP_{75} are obtained at the single IoU threshold 0.5 and 0.75 over all categories. AP is obtained by averaging over threshold 0.5 to 0.95 over all categories.

4.3. Input image resolution adjustment

We identified the image size of (928×928) as yielding the highest performance in AP_{50} , AP , and Recall.

Table 2: Performance comparison across image size

Input image resolution	AP_{50}	AP	Recall	Precision
(640×640)	0.621	0.436	0.539	0.796
(800×800)	0.665	0.489	0.583	0.821
(928×928) ✓	0.696	0.525	0.613	0.819

4.4. Data augmentation

A total of three of different augmentation packages were tested and the implemented augmentation types were explained in Table 3. **Default** denotes default augmentation setting provided by the Ultralytics, **Geo** denotes geometric transformations, and **Color** denotes HSV color space adjustment. The exact augmentations are provided in the repository.

Table 3: Performance metrics across augmentation

Package	Default	Geo	Color	AP_{50}	AP	Recall	Precision
Ver 1 ✓	✓			0.621	0.436	0.539	0.796
Ver 2	✓	✓		0.604	0.416	0.530	0.763
Ver 3	✓		✓	0.616	0.428	0.536	0.786

4.5. Attention & gating mechanism

A total of six attention-augmented backbones were tested in Table 4 and the designs are displayed in Figure 2. Dotted lines are used to distinguish between backbones employing single-type versus multiple-type modules. In the trainings

using modified DOTA, the third design outperformed other candidates. The top 3 candidates were then trained with VisDrone dataset to check performance and the second design (Only-CBAM) achieved the highest accuracy.

The third design: Although the third design failed to obtain the best performance when trained using VisDrone, we decided to use the third design for the final training configuration since it edges out other backbones when trained with DOTA. We name this particular backbone with SE Block-CBAM arrangement as **Mixture of Orthogonal Neural-modules Network(MoonNet)**.

Unfortunately, identity-safe gating ($1 + \tanh(\cdot)$) failed to achieve enhancement when trained with YOLO models. Thus, we did not run additional trainings using tanh gating when using VisDrone. However, tanh gate achieved enhancement when adapted to YOLC framework in Table 7 and 8.

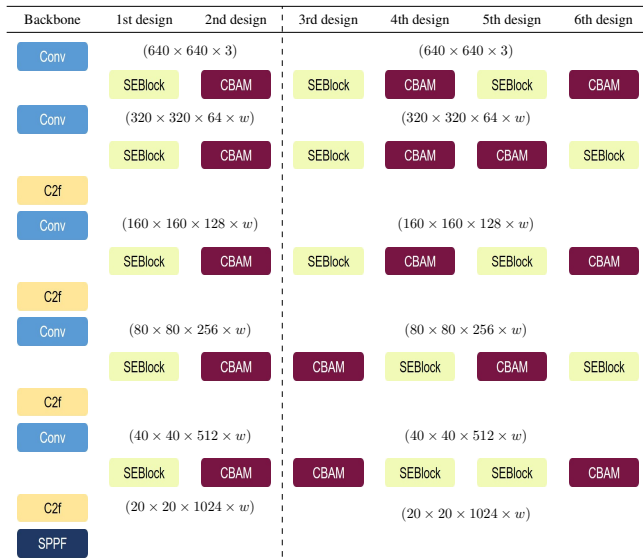


Fig. 2: Backbone designs

Table 4: Backbone results

Backbone	sigmoid	1+tanh	AP_{50}	AP	Recall	Precision
Dataset: Modified DOTAv2.0 (50 epochs)						
Default	no attention		0.486	0.299	0.427	0.690
1st Design	✓		0.491	0.301	0.437	0.685
2nd Design	✓	✓	0.471	0.287	0.417	0.700
3rd Design	✓	✓	0.489	0.299	0.433	0.702
4th Design	✓	✓	0.467	0.279	0.415	0.702
5th Design	✓	✓	0.503	0.313	0.444	0.697
6th Design	✓	✓	0.490	0.300	0.430	0.702
1st Design	✓		0.483	0.294	0.441	0.681
2nd Design	✓	✓	0.473	0.289	0.427	0.680
3rd Design	✓	✓	0.483	0.293	0.425	0.706
4th Design	✓	✓	0.472	0.286	0.424	0.682
5th Design	✓	✓	0.485	0.297	0.434	0.685
6th Design	✓	✓	0.471	0.282	0.422	0.677
Dataset: VisDrone (50 epochs)						
1st Design	✓		0.294	0.170	0.303	0.414
2nd Design	✓	✓	0.296	0.172	0.304	0.412
3rd Design	✓		0.293	0.169	0.303	0.409

4.6. Final training and integration with YOLC

The final MoonNet-based model was trained from scratch with optimized input image resolutions and augmentations, showing clear improvements over the default YOLOv8n. In Table 5, **Default** refers to the original backbone, **Res** to optimized input image resolution, and **Aug** to optimized augmentations. The number of channels from the model’s backbone in the final training is not identical to the numbers presented in Table 4. This is because all the final trainings in the Table 5 were conducted using YOLOv8n model scale thus actual number of channels were (16, 32, 64, 128, 256) due to the channel multiplier (0.25). In Table 6, all parameters from preprocess to end-to-end are measured in milliseconds.

Table 5: Performance metrics for final models

Method	Default	MoonNet	Res	Aug	AP_{50}	AP	Recall	Precision
Method 1	✓				0.491	0.308	0.390	0.685
Method 2	✓		✓		0.596	0.411	0.501	0.763
Method 3	✓		✓	✓	0.664	0.485	0.565	0.843
Method 4		✓	✓	✓	0.667	0.486	0.566	0.849

Table 6: GFLOPs and latency comparison

Method	GFLOPs	Preprocess	Inference	Postprocess	End-to-End
Method 1	8.3	0.1	1.9	2.3	4.3
Method 2	8.3	0.2	2.2	2.6	5.0
Method 3	8.3	0.2	2.2	2.7	5.1
Method 4	8.4	0.2	2.6	2.4	5.2

The MoonNet’s (SE Block–CBAM) orientation is then adapted to the YOLC framework to check the MoonNet’s adaptability and enhancement potential. MoonNet (sigmoid) and MoonNet (1+tanh) both achieved improved results compare to the original YOLC in Table 7. The MoonNet (1+tanh) achieved +6.13% gain in AP and +3.77% gain in AP_{50} compare to the MoonNet (sigmoid).

Table 7: The state-of-the-art comparison on VisDrone

Method	Backbone	AP	AP_{50}	AP_{75}
ClusDet[21]	ResNet101	0.267	0.504	0.252
ClusDet[21]	ResNeXt101	0.284	0.532	0.264
DMNet [22]	ResNet101	0.285	0.481	0.294
DMNet [22]	ResNext101	0.294	0.493	0.306
YOLO(k=1) [12]	HRNet	0.303	0.516	0.307
YOLO(k=1)(Ours)	HRNet + MoonNet(sigmoid)	0.310	0.530	0.311
YOLO(k=1)(Ours)	HRNet + MoonNet(1+tanh)	0.329	0.550	0.336

Table 8: Gating mechanism comparison

Framework	sigmoid	1+tanh	AP_{50}	AP
YOLO-MoonNet (DOTA)	✓	✓	0.503	0.313
YOLO-MoonNet (DOTA)		✓	0.490	0.300
YOLO-MoonNet (VisDrone)		✓	0.310	0.530
YOLO-MoonNet (VisDrone)	✓	✓	0.329	0.550

4.7. Ablation Study

Image resolution adjustment (*Method1* \rightarrow *Method2*)

Varying the input image resolution yields +21.38% gain in AP_{50} and +33.44% gain in AP showing improved optimization helps recover missed tiny objects.

Proper data augmentation (*Method2* \rightarrow *Method3*)

Instead of adding excessive geometric transformations such as rotation and color space adjustment, mild use of augmentations leads to +11.41% gain in AP_{50} and +18% gain in AP .

Effectiveness of MoonNet (*Method3* \rightarrow *Method4*)

Compared to the previous two steps, replacement of the backbone from vanilla CSP to MoonNet yields lower increment. +0.45% gain in AP_{50} and +0.21% gain in AP , but obtained the highest scores: 0.667 AP_{50} and 0.486 AP .

Computational burden (*GFLOPs and latency*)

For the training using the final configuration, only 0.1 increase in GFLOPs and 0.9 ms increase were measured from the base score in Table 6 which highlights MoonNet’s high deployability with small costs.

Hybrid use of attention modules (*SE Block & CBAM*)

Our third design MoonNet which consists of multiple attention modules demonstrated significant enhancement in detection performance. However, the power of multi-use of attention modules is still questionable. In Table 4, design 4, 5 and 6 also used SE Block and CBAM together but failed to achieve higher metrics than the designs with single-type attention module. MoonNet’s SE Block orientation in the early layer and CBAM in the later stage conveys that the channel emphasis from SE Block followed by spatial focus from CBAM can be particularly effective for combined use of multiple attention modules. When using more than one attention module within a single backbone, careful consideration in module arrangement is required.

Adaptability of MoonNet (*YOLOC integration*)

In Table 7, the MoonNet’s attention module arrangement was integrated into the YOLC model with two different gating

functions and achieved state-of-the-art performance when compared with ClusDet[21] and DMNet[22], both trained on cluster-aware cropped images. Ours(sigmoid) obtained +16.10% gain in AP compared to ClusDet, +8.77% gain compared to DMNet and +2.31% gain against the original YOLC. Ours(1+tanh) obtained +23.22% gain in AP compared to ClusDet, +15.44% gain compared to DMNet and +8.58% gain against the original YOLC.

Alternative gating mechanism ($1 + \tanh()$)

An attention module’s gating mechanism is framework-dependent and this is evident through Table 8’s result. In YOLC framework (HRNet), identity safe gating using tanh might be a better option. Our ablation also revealed that the identity safe gating is unnecessary for the YOLO (CSPDarknet) framework. Therefore, careful consideration on choosing gate function is essential.

4.8. Visual predictions

Visual predictions were made in Figure 3. As the method evolves from 1 to 4, the model begins to capture more small vehicles, and the method 4 model correctly performs separate detection of small and large vehicles. YOLC+MoonNet model also demonstrates better detection performance.

5. CONCLUSION

This research improves tiny object detection by combining resolution adjustment, augmentation, and the MoonNet backbone with tanh gating function. Compared to the base YOLOv8n-obb model, the final model (Method 4) achieved gains of +35.85% AP_{50} , +57.79% AP , +45.13% recall, and +23.94% precision. Moreover, the MoonNet-integrated backbone achieved state-of-the-art performance among the cluster-aware detectors confirming an attention-augmented backbone enhances detection of small targets in aerial imagery. However, the multiple use of attention modules cannot guarantee consistent enhancement. Its orientation and gating function need to be tuned for the appropriate implementation.

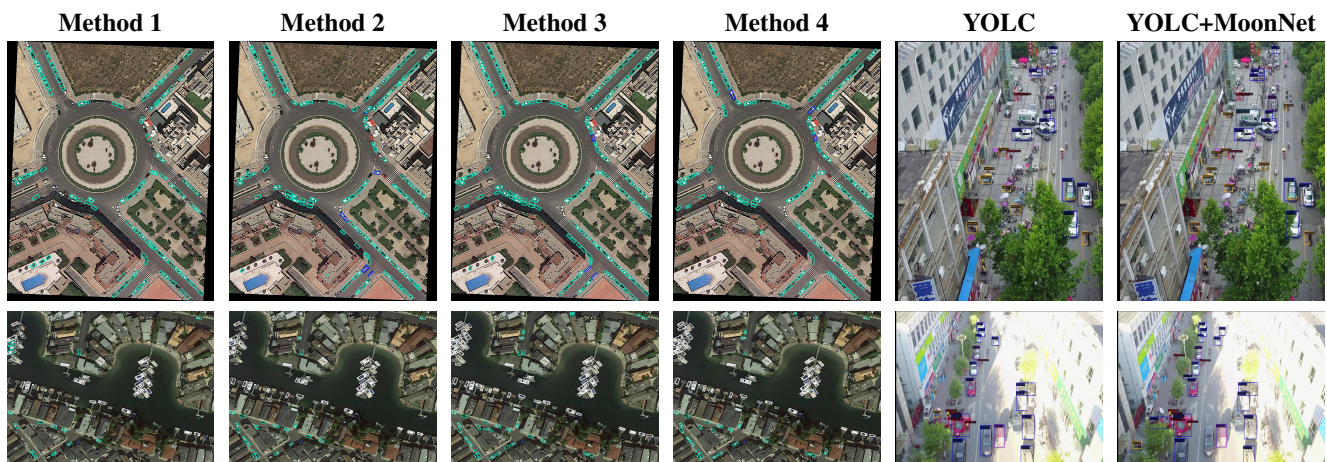


Fig. 3: Visual comparison of detection performance on tiny objects across two different aerial scenes.

6. REFERENCES

- [1] Ross Girshick, Jeff Donahue, Trevor Darrell, and Jitendra Malik, “Rich feature hierarchies for accurate object detection and semantic segmentation,” in *CVPR*, 2014, pp. 580–587.
- [2] Shaoqing Ren, Kaiming He, Ross Girshick, and Jian Sun, “Faster R-CNN: Towards real-time object detection with region proposal networks,” in *NeurIPS*, 2015, pp. 91–99.
- [3] Tsung-Yi Lin, Piotr Dollár, Ross Girshick, Kaiming He, Bharath Hariharan, and Serge Belongie, “Feature pyramid networks for object detection,” in *CVPR*, 2017, pp. 2117–2125.
- [4] Kaiming He, Georgia Gkioxari, Piotr Dollár, and Ross Girshick, “Mask R-CNN,” in *ICCV*, 2017, pp. 2961–2969.
- [5] Wei Liu, Dragomir Anguelov, Dumitru Erhan, Christian Szegedy, Scott Reed, Cheng-Yang Fu, and Alexander C. Berg, “SSD: Single shot multibox detector,” in *ECCV*, 2016, pp. 21–37.
- [6] Joseph Redmon, Santosh Divvala, Ross Girshick, and Ali Farhadi, “You only look once: Unified, real-time object detection,” 2016, vol. 2016-December.
- [7] Joseph Redmon and Ali Farhadi, “YOLOv3: An incremental improvement,” in *arXiv preprint arXiv:1804.02767*, 2018.
- [8] Xingkui Zhu, Shuchang Lyu, Xu Wang, and Qi Zhao, “Tph-yolov5: Improved yolov5 based on transformer prediction head for object detection on drone-captured scenarios,” in *Proceedings of the IEEE/CVF International Conference on Computer Vision (ICCV) Workshops*, October 2021, pp. 2778–2788.
- [9] Zhenping Kang, Yurong Liao, Shuhan Du, Haonan Li, and Zhaoming Li, “Se-cbam-yolov7: An improved lightweight attention mechanism-based yolov7 for real-time detection of small aircraft targets in microsatellite remote sensing imaging,” *Aerospace*, vol. 11, no. 8, pp. 605, 2024.
- [10] Chang Xu, Jinwang Wang, Wen Yang, Huai Yu, Lei Yu, and Gui-Song Xia, “Detecting tiny objects in aerial images: A normalized wasserstein distance and a new benchmark,” *ISPRS Journal of Photogrammetry and Remote Sensing*, vol. 190, pp. 79–93, 2022.
- [11] Chenhongyi Yang, Zehao Huang, and Naiyan Wang, “Querydet: Cascaded sparse query for accelerating high-resolution small object detection,” in *CVPR*, 2022, pp. 13658–13667.
- [12] Chenguang Liu, Guangshuai Gao, Ziyue Huang, Zhenghui Hu, Qingjie Liu, and Yunhong Wang, “Yolc: You only look clusters for tiny object detection in aerial images,” *IEEE Transactions on Intelligent Transportation Systems*, vol. 25, no. 10, pp. 13863–13875, 2024.
- [13] Longbin Yan, Yunxiao Qin, and Jie Chen, “Scale-balanced real-time object detection with varying input-image resolution,” *IEEE Transactions on Circuits and Systems for Video Technology*, vol. 33, pp. 242–256, 1 2023.
- [14] Mate Kisantal, Zbigniew Wojna, Jakub Murawski, Jacek Naruniec, and Kyunghyun Cho, “Augmentation for small object detection,” 2019.
- [15] Jie Hu, Li Shen, Samuel Albanie, Gang Sun, and Enhua Wu, “Squeeze-and-excitation networks,” *IEEE Transactions on Pattern Analysis and Machine Intelligence*, vol. 42, 2020.
- [16] Sanghyun Woo, Jongchan Park, Joon Young Lee, and In So Kweon, “Cbam: Convolutional block attention module,” 2018, vol. 11211 LNCS.
- [17] Mingyang Ma and Huanli Pang, “Sp-yolov8s: An improved yolov8s model for remote sensing image tiny object detection,” *Applied Sciences*, vol. 13, no. 14, pp. 8161, 2023.
- [18] Mengzi Hu, Ziyang Li, Jiong Yu, Xueqiang Wan, Haotian Tan, and Zeyu Lin, “Efficient-lightweight yolo: Improving small object detection in yolo for aerial images,” *Sensors*, vol. 23, no. 14, pp. 6423, 2023.
- [19] Qilong Wang, Banggu Wu, Pengfei Zhu, Peihua Li, Wangmeng Zuo, and Qinghua Hu, “Eca-net: Efficient channel attention for deep convolutional neural networks,” in *The IEEE Conference on Computer Vision and Pattern Recognition (CVPR)*, 2020.
- [20] Tsung-Yi Lin, Michael Maire, Serge Belongie, James Hays, Pietro Perona, Deva Ramanan, Piotr Dollár, and C. Lawrence Zitnick, “Microsoft COCO: Common objects in context,” in *ECCV*. 2014, pp. 740–755, Springer.
- [21] Fan Yang, Heng Fan, Peng Chu, Erik Blasch, and Haibin Ling, “Clustered object detection in aerial images,” in *ICCV*, October 2019, pp. 8310–8319.
- [22] Changlin Li, Taojiannan Yang, Sijie Zhu, Chen Chen, and Shanyue Guan, “Density map guided object detection in aerial images,” in *CVPRW*, 2020, pp. 737–746.